Journal of Power Sources 445 (2020) 227327

Contents lists available at ScienceDirect

Journal of Power Sources

journal homepage: www.elsevier.com/locate/jpowsour

The role of A-site ion on proton diffusion in perovskite oxides (ABO_3)

Yuhang Jing [a,b,*], N.R. Aluru [b,c]

[a] Department of Astronautical Science and Mechanics, Harbin Institute of Technology, Harbin, Heilongjiang, 150001, PR China
[b] Beckman Institute for Advanced Science and Technology, National Center for Supercomputing Applications (NCSA), University of Illinois at Urbana-Champaign, Urbana, IL, 61801, USA
[c] Department of Mechanical Science and Engineering, University of Illinois at Urbana-Champaign, Urbana, IL, 61801, USA

HIGHLIGHTS

- The energy barriers of proton diffusion are decomposed.
- The local lattice deformations play a significant role in proton diffusion.
- The migration energies of proton diffusion near an A ion vacancy are large.
- The A-site ion in a perovskite oxide can reduce the B-O bond strength.
- The A-site ion in a perovskite oxide facilitate local lattice deformations.

ARTICLE INFO

Keywords:
Proton diffusion
Perovskite oxide
Lattice deformation
Origin of energy barrier
Density functional theory calculation

ABSTRACT

By performing detailed density functional theory (DFT) calculations, we investigate the effect of A ion vacancy on both hydroxide ion rotation and proton transfer in Y-doped $BaZrO_3$. We find that A ions reduce the barrier for proton diffusion in a perovskite oxide, demonstrating the significance of perovskite structures as proton conductors. Proton diffusion is understood as a two-step mechanism consisting of hydroxide ion rotation and proton transfer. In both steps, lattice deformations play an important role – specifically, the outward O-B-O bending and A ion motions are important for hydroxide ion rotation, and inward O-B-O bending facilitates proton transfer. By comparing the bond strength, we reveal that an A ion can reduce the bond strength of O and B ion, thereby reducing the energy barrier for local lattice deformation such as O-B-O bending motion, which facilitates both hydroxide ion rotation and proton transfer. Our analysis provides a detailed atomistic understanding of the role of A-site ion on proton diffusion in perovskite oxides. The study presented here not only indicates the advantage of perovskite oxides as proton conductors but also elucidates the origin of proton diffusion barrier which can pave the way for design of novel proton conductors.

1. Introduction

Perovskite oxides [1] have received great attention due to their interesting properties including ferroelectricity [2], piezoelectricity [3], ionic conductivity [4], mixed ionic and electronic conductivity [5], high-temperature superconductivity [6], thermal stability [7], and catalytic properties [8]. In particular, significant proton conductivity combined with good chemical and mechanical stability of acceptor-doped perovskite oxides make them promising candidates as electrolytes for intermediate-temperature solid oxide fuel cells [9,10,48] and electrolysis cells [11]. For example, yttrium-doped barium zirconate which has an excellent crystalline quality has been shown to have a bulk proton conductivity of 0.11 S cm^{-1} at 500 °C, which is significantly larger than the conductivity of oxide-ion conducting electrolytes in the same temperature range [12]. However, the high surface reactivity of some barium-based perovskites with H_2O leads to the formation of protonic species at the sample surface by corrosion preventing their usage in industrial applications such as in energy production systems [41–43]. Therefore, prior to investigation of proton dynamics, one should differentiate surface and bulk protons. In order to deal with bulk protons, neutron measurements should be performed on single crystals and homogeneous, dense perovskite oxides (more than 95% of the theoretical density). Additionally, it is difficult to identify and locate protons in various proton conductors [47], especially at a temperature

* Corresponding author. Department of Astronautical Science and Mechanics, Harbin Institute of Technology, Harbin, Heilongjiang, 150001, PR China.
E-mail address: jingyh@hit.edu.cn (Y. Jing).

https://doi.org/10.1016/j.jpowsour.2019.227327
Received 1 August 2019; Received in revised form 25 September 2019; Accepted 16 October 2019
Available online 23 October 2019
0378-7753/

range where proton conductivity is observed. Consequently, some forms of protons (free/ballistic/polaronic protons) have been proposed [44–46]. For instance, the observation of broad bands between 2000 and 3500 cm^{-1} from the IR spectra in partially substituted barium zirconate perovskites has been assigned to the OH group with strong H-bonds and the mechanism was modeled, while different mechanisms including polaronic protons were proposed for some other proton conductors. To our knowledge, however, there is no significant literature on the origin of the activation energy of proton transport in single-crystalline perovskites, where excellent proton conductivity is mainly attributed to the lower activation energy for proton transport in perovskite oxides compared to the oxide ion transport in conventional oxide-ion conducting electrolytes [10]. Although the proton transport mechanisms in perovskite oxides have been explored [13–17], the mechanisms governing lower activation energy of proton diffusion in single-crystalline pervoskite oxides remain unclear. Therefore, the design and development of novel proton conducting solid oxide electrolytes with high conductivity remains a significant challenge.

Perovskite oxides have a typical chemical formula of ABO_3, where A and B are two different cations. Generally, the B-site cations are six-fold coordinated with oxygen atoms to form corner sharing BO_6-octahedrons, while the A-site cations occupy the voids created by the octahedrons. Although a few perovskite oxides have an ideal cubic lattice, many perovskite oxides are slightly distorted with a lower symmetry (e.g. orthorhombic) measured by the tolerance factor[1], $t = \frac{R_A+R_O}{\sqrt{2}(R_B+R_O)}$ where R_A, R_B and R_O are the ionic radii of the A, B site cations and oxide ion, respectively. Under humid conditions, protons are incorporated into acceptor-doped perovskite oxides [18–20]. Proton diffusion in perovskite oxides is generally characterized by a Grotthuss mechanism [36] involving proton transfer between two neighboring oxide ions belonging to the same BO_6-octahedron (intraoctahedral proton transfer) or between two oxide ions belonging to two neighboring BO_6-octahedrons (interoctahedral proton transfer) and hydroxide ion rotation [10,18] as shown in Fig. 1 (Top left). The elementary events underlying proton transfer and hydroxide ion rotation have been investigated by both experiments [17,21] and computations [10,13,22–24]. Quantum molecular dynamics simulations have shown that the proton transfer is related to lattice dynamics with the coupling of proton transfer to the O-B-O bending mode [13]. The rate limiting step in proton conductivity is identified to be the proton transfer rather than the rapid hydroxyl ion reorientation which requires a very small activation energy. However, recent experimental work [17] has shown that the interaction of protons with the crystal lattice and proton-phonon coupling is important and proton motion at high temperature can be described by the Samgin's proton polaron model; in addition, O-Ce-O bending mode has been shown to be not as significant as Ce-O stretching mode which is considered to cause the coupling of the low-energy phonon mode with the proton diffusion and thus contribute to proton transport in yttrium-doped barium cerate. In addition to this coupling between lattice dynamics and proton transport, a key question that hasn't been addressed regarding proton transport is the role of A-site ions on proton diffusion in perovskite oxides, i.e., why do good proton conductors have the ABO_3 perovskite structure instead of, for example, the BO_3 structure with BO_6-octahedrons? It is well known that the structural property and electronic conductivity of perovskite oxides can be tailored to specific applications by substituting A cations by dopants [49–51]. However, how A-site ions affect the lattice dynamics of perovskite oxides is unknown. Although previous experimental results [25,26] have shown that A-site ion's deficiency in doped BaZrO3 and BaCeO3 proton-conducting systems has a strong influence on proton conductivity, the reasons were not clear. Clear insights can be obtained by analyzing the role of A-site ions on the proton diffusion mechanism, i.e., by considering the elementary steps underlying the proton transfer, hydroxide ion rotation, and the coupling of lattice dynamics to hydroxide ion rotation, which does not have a negligible barrier as shown in ref [27].

In this paper, we perform density functional theory (DFT) calculations to address two key questions: (1) the origin of the activation energy for hydroxide ion rotation and proton transfer, and (2) the role of A-site ion on proton diffusion in perovskite oxides. Our results indicate that outward O-B-O bending motion weakens hydrogen bond, and gives rise to hydroxide ion reorientation in AO plane while inward O-B-O bending motion induces hydroxide ion rotation out of AO plane, and then strengthens hydrogen bond which governs the O_D-H-O_A interactions. The details of proton diffusion mechanism in perovskite oxides are shown in Fig. 1 (middle four figures in both rows). Furthermore, the A-site ion in a perovskite oxide can reduce the B-O bond strength, thereby reducing the energy barrier for local lattice deformations, such as the O-B-O bending motion, and the B-O-B bending motion (Top right and bottom right figures), which helps both the hydroxide ion rotation and proton transfer. To our knowledge, this is the first systematic study on the origin of activation energy of proton transfer and hydroxide ion rotation, and the role of A-site ion, providing a deep understanding of the advantage of perovskite oxide as a proton conductor.

2. Computational details

All DFT calculations are performed using the Vienna Ab initio

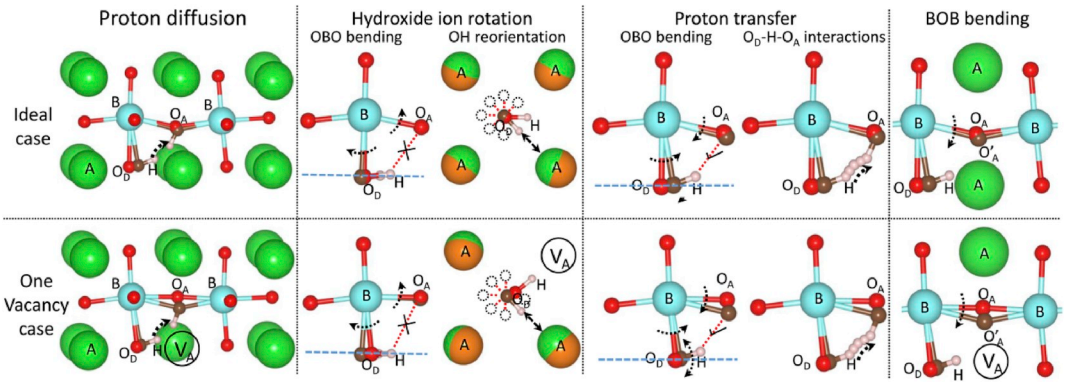

Fig. 1. Schematic illustration of the proton diffusion mechanism in an ABO_3 perovskite oxide without (top row) and with (bottom row) one A ion vacancy. Top left and bottom left figures show the proton diffusion mechanism in 3D structures: hydroxide ion rotation in AO plane and proton transfer in BO_2 plane. Middle four figures in both rows describe the elementary steps underlying hydroxide ion rotation: outward O-B-O bending motion and hydroxide ion reorientation in AO plane, and proton transfer: inward O-B-O bending motion, hydroxide ion rotation out of AO plane, and O_D-H-O_A interactions in BO_2 plane. Top right and bottom right figures show additional B-O-B bending motion involved in both hydroxide ion rotation and proton transfer. The red balls denote the initial positions and the brown balls show the final positions. (For interpretation of the references to colour in this figure legend, the reader is referred to the Web version of this article.)

simulation package (VASP) [28–30] with the projector augmented wave (PAW) method [30]. The Perdew-Burke-Ernzerhof (PBE) [31] exchange-correlation functional is used. The cutoff energy for the plane wave basis set for all calculations is 500 eV which has been used for proton conducting perovskites [19,39]. All atoms are relaxed using the conjugate gradient method until the forces on each atom are less than 0.02 eV/Å. All the calculations are non spin-polarized. The migration energy barriers are calculated using the climbing image nudged elastic band (CI-NEB) method [32]. The bond strength between atoms can be characterized by bond order. The density derived electrostatic and chemical (DDEC6) approach [35] is thus performed to calculate the electronic density overlap populations (bond orders) between two atoms.

Y-doped $BaZrO_3$ (BZY) is one of the most promising proton-conducting perovskites. We first focus on this perovskite to understand the role of A-site ion on proton diffusion. In addition, in order to clarify the origin of proton diffusion including proton transfer and hydroxide ion rotation, several orthorhombic and cubic perovskites are considered. The popular Sr-, Ba-, and La-based perovskites are chosen and BO3 structures such as UO3 are also studied. The unit cell volume of perovskites varies with different B-site cations. The cubic and orthorhombic unit cells are optimized using a $6 \times 6 \times 4$ and a $6 \times 6 \times 6$ Monkhorst-Pack k-points mesh, respectively. Based on the optimized unit cell, a supercell with $2 \times 2 \times 2$ orthorhombic unit cells and a supercell with $3 \times 3 \times 3$ cubic unit cells are constructed and optimized. Next, following experimental results[1], one oxide ion vacancy is introduced in the supercell with two B-site ions substituted with two dopants which have a lower valence and a slightly larger ionic size than the original B-site ion. The preferred positions of the two dopants and the oxide ion vacancy are obtained by locating them at different atomic sites and comparing the total energies of the system. After obtaining the bulk acceptor-doped perovskite oxides, one water molecule is incorporated into the system and two protons are introduced. In all calculations, only one proton's motion is considered while the second proton is bonded to the initial oxygen and relaxed freely. $2 \times 2 \times 2$ Monkhorst-Pack k-points mesh is used for bulk calculations. To investigate the role of A-site ion on proton diffusion, one A ion vacancy or two A ion vacancies close to the proton are introduced in the supercell, and one O ion vacancy or two O ion vacancies far away from the A ion vacancy are created to make the system neutral. The local configurations of the three optimized systems are shown in Fig. S1.

3. Results and discussion

3.1. Activation energy for hydroxide ion rotation

To understand the origin of the activation energy for hydroxide ion rotation, we performed NEB calculations to estimate the energy barriers for hydroxide ion rotation in the AO plane. The relative energy in the NEB trajectory for one BZY system (top snapshots in Fig. S2) is shown in Fig. 2a. The energy barrier for hydroxide ion rotation is 0.196 eV. To confirm this result, different hydroxide ion rotations are considered. The

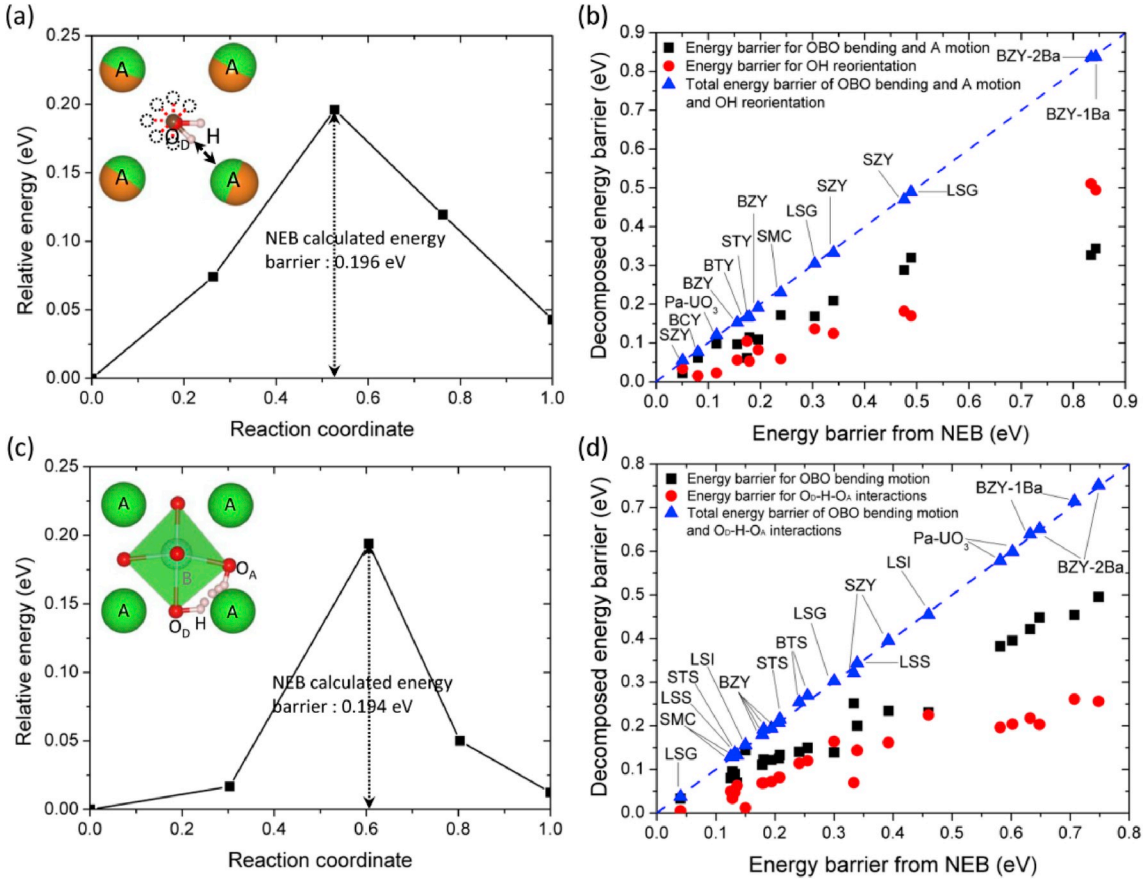

Fig. 2. (a) Total energy barrier for the hydroxide ion rotation in the AO plane of a perovskite oxide. (b) Decomposed energy barrier for the hydroxide ion rotation vs. NEB calculated energy barriers for different oxides. (c) Total energy barrier for the proton transfer in a perovskite oxide. (d) Decomposed energy barrier for proton transfer vs. NEB calculated energy barrier for different oxides. BZY: Yttrium-doped Barium Zirconate, BZY-1Ba: Yttrium-doped Barium Zirconate with one A ion vacancy, BZY-2Ba: Yttrium-doped Barium Zirconate with two A ion vacancies, SZY: Yttrium-doped Strontium Zirconate, BTY: Yttrium-doped Barium Titanate, BTS: Scandium-doped Barium Titanate, STY: Yttrium-doped Strontium Titanate, STS: Yttrium-doped Barium Titanate, SMC: Chromium-doped Strontium Manganate, BCY: Yttrium-doped Barium Cerate, LSG: Strontium-doped Lanthanum Gallium Oxide, LSI: Strontium-doped Lanthanum Indium Oxide, LSS: Strontium-doped Lanthanum Scandium Oxide, Pa-UO_3: Protactinium-doped Uranium Oxide.

results are shown in Table S1. It can be seen that the calculated barriers of 0.16–0.196 eV for hydroxide ion rotation in a perfect BZY are consistent with previous theoretical calculations [33,34]. The barriers for hydroxide ion rotation are comparable to those of proton transfer [34] which has been identified as the rate limiting step in proton conductivity. In order to understand the origin of the energy barrier for hydroxide ion rotation, lattice deformations between initial and saddle structures (the structures with maximum energy barriers) are studied and the three elementary steps underlying the hydroxide ion rotation are suggested: these are (1) outward O-B-O bending motion weakening hydrogen bond (H-O_A bond in the middle plot under hydroxide ion rotation column of Fig. 1) and A ion motion, (2) hydroxide ion reorientation in the AO plane, and (3) lattice relaxation towards its lower energy configuration. The relative energy associated with these three elementary steps is shown in Fig. 3a–c and detailed calculation processes are described in Figs. S3a–c. Fig. 3a shows the relative energy with the O-B-O bending angle (∠ O_DBO_A of inset figure). The energy barrier associated with this lattice deformation is 0.109 eV. Fig. 3b shows the relative energy of hydroxide ion reorientation in the AO plane. The relative energy increases and reaches the maximum when the hydroxide ion is oriented towards the A ion (see the inset of Fig. 3b) because of the repulsion between A ion and proton, and then decreases as the hydroxide ion further rotates to a new favorable orientation. The energy barrier of this movement is 0.083 eV. Fig. 3c shows the relative energy with the O-B-O bending angle (∠ O_DZrO_C in Fig. S2) during lattice relaxation. There is no energy barrier associated with this process as the deformed lattice relaxes back towards its lower energy configuration. It can be noticed that the energy barrier associated with the hydroxide ion rotation based on its decomposition into the first two processes is 0.192 eV (Fig. 3b), which is consistent with the NEB calculated result of 0.196 eV (Fig. 2a). To further quantify the importance and contribution of these two steps, a few other perovskite oxides with different unit-cell volumes and one metal trioxide are investigated. The NEB calculated hydroxide ion rotation barriers and the energy barriers associated with outward O-B-O bending and A ion motions and hydroxide ion reorientation are summarized in Fig. 2b. We note that the sum of the decomposed energy barriers is consistent with NEB results, implying that the decomposition of the total energy barrier into O-B-O bending and A ion motions and hydroxide ion reorientation provides good insights on the activation energy for hydroxide ion rotation. These results also suggest that the local lattice deformations play a significant role in the hydroxide ion rotation.

3.2. Activation energy for proton transfer

While the importance of the O-B-O bending mode to proton transfer has been mentioned before [13], the precise contribution and coupling of the O-B-O bending mode to proton transfer barrier has not been quantified. We performed NEB calculations to estimate the energy barrier for a proton transfer from an oxygen donor (O_D) to an oxygen acceptor (O_A) as shown in Fig. 1 (top left). The relative energy in the NEB trajectory for one BZY system (top snapshots in Fig. S4) is shown in Fig. 2c. The energy barrier for the proton transfer is 0.194 eV, which is consistent with previous experiment [15] and theoretical calculations [33,34,40]. By analyzing the lattice deformations between initial and saddle structures, three elementary steps underlying the proton transfer are suggested: these are (1) inward O-B-O bending motion causing hydroxide ion rotational motion out of the AO plane due to hydrogen bond (H-O_A bond in the middle plot under proton transfer column of Fig. 1), (2) O_D-H-O_A interactions, and (3) recovery of the O-B-O bending motion. The calculated energy barrier for the hydroxide ion rotation out of the AO plane (shown in the middle plot under proton transfer column of Fig. 1) is about 0.02 eV agreeing with previous theoretical calculations [33]. Since this is a negligible barrier, the hydroxide ion rotation out of

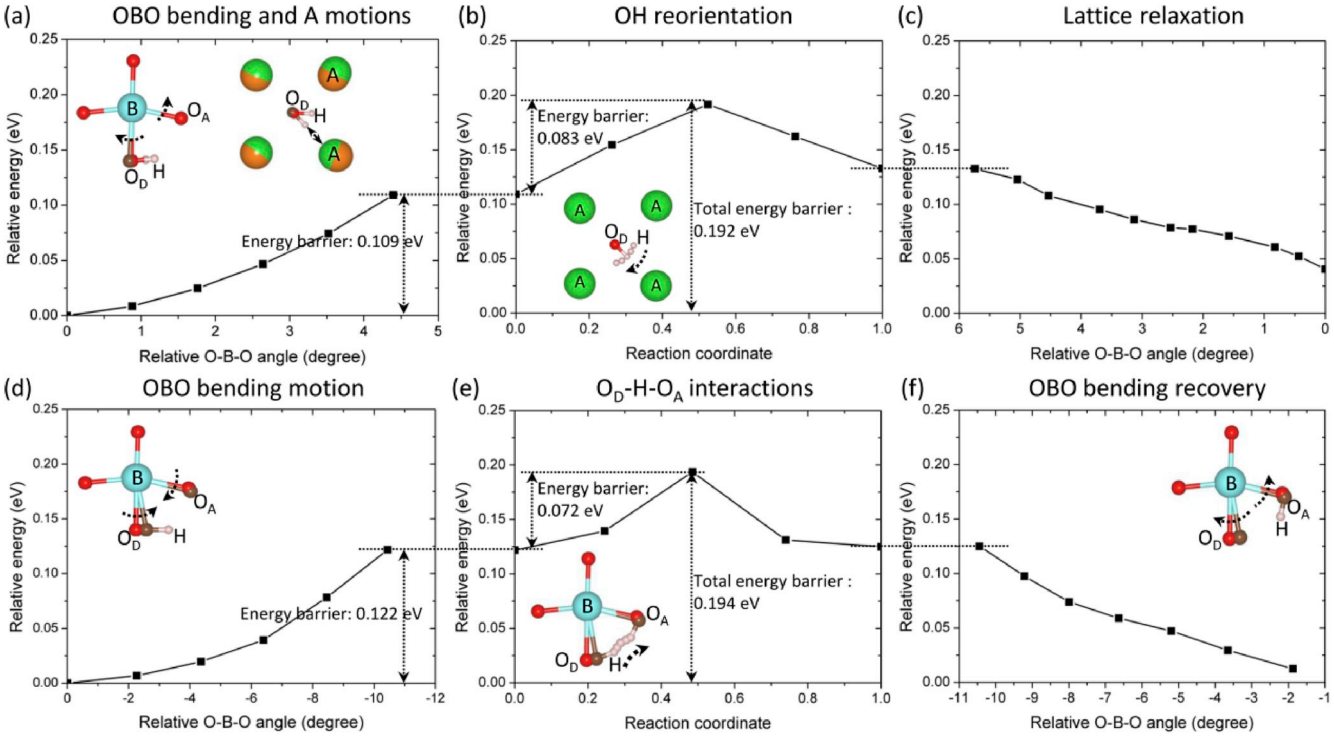

Fig. 3. Three elementary steps underlying the hydroxide ion rotation and proton transfer in BZY. (a) Relative energy with the O-B-O bending angle (∠ O_DBO_A of inset figure) during the outward O-B-O bending and A ion motions. (b) Relative energy with hydroxide ion reorientation in AO plane. (c) Relative energy with the O-B-O bending angle (∠ O_DZrO_C in Fig. S2) during lattice relaxation. (d) Relative energy with the O-B-O bending angle (∠ O_DBO_A of inset figure) during the inward O-B-O bending. (e) Relative energy for O_D-H-O_A interactions. (f) Relative energy with the O-B-O bending angle (∠ O_DBO_A of inset figure) during the recovery of the O-B-O bending motion. Inset figures show the local lattice deformation of saddle structure compared to initial structure. The red balls denote the initial positions and the brown balls show the final positions. (For interpretation of the references to colour in this figure legend, the reader is referred to the Web version of this article.)

the AO plane is not considered as an elementary step during proton transfer. The relative energy associated with these three elementary steps is shown in Fig. 3d–f and detailed calculation processes are described in Figs. S3d–f. Fig. 3d shows the relative energy with the O-B-O bending angle (∠ O_DBO_A of inset figure). The energy barrier of this lattice deformation is 0.122 eV. Fig. 3e shows the relative energy for O_D-H-O_A interactions. The relative energy increases and reaches the maximum when the proton is in the middle of O_D and O_A, and then decreases as proton approaches O_A. The energy barrier of this motion is 0.072 eV. Fig. 3f shows the relative energy with the relaxation of the O-B-O bending angle (∠ O_DBO_A of inset figure). There is no energy barrier because this process mainly involves lattice relaxation to recover the original O-B-O angle. It can be noticed that the energy barrier associated with proton transfer based on its decomposition into the first two processes is 0.194 eV (Fig. 3e), which is equal to the NEB calculated result of 0.194 eV (Fig. 2c). Similar to the hydroxide ion rotation case, a few other perovskite oxides with different unit-cell volumes and one metal trioxide are investigated to further quantify the importance and contribution of these two processes. The NEB calculated proton transfer barriers and the energy barriers associated with inward O-B-O bending motion and O_D-H-O_A interactions are summarized in Fig. 2d. We note that the sum of the decomposed energy barriers is consistent with NEB results for proton transfer. The energy barriers associated with O-B-O bending motion are larger than those for O_D-H-O_A interactions, indicating that local lattice deformations govern proton transfer.

It is important to note that the energy barriers should be calculated using the Gibbs free energy. The total energy obtained from DFT does not account for the entropic contribution. However, the entropic contribution to the energy barrier is small [52,53]. We also note that it is often assumed that proton tunneling is much less important in perovskites than in metals [54]. Therefore, the origin of activation energy is revealed in the current work without considering the temperature effects.

3.3. Role of A-site ions on hydroxide ion rotation

To investigate the role of A-site ions, the hydroxide ion rotation in three systems (ideal structure with no A ion vacancies, one A ion vacancy, and two A ion vacancies) shown in Fig. S1 is compared with NEB calculations. The relative energies in the NEB trajectories (snapshots in Fig. S2) are shown in Fig. 4a. It can be seen that the energy barriers for a hydroxide ion rotation near an A ion vacancy are significantly higher than that in the perfect lattice. To confirm this result, different hydroxide ion rotations near or far away from dopants (shown in Fig. S5) are considered. The energy barriers are summarized in Table S1. We note that the barriers of 0.83–0.98 eV for a hydroxide ion rotation near an A ion vacancy are larger than those in the perfect lattice. We can thus conclude that the effect of the A ion vacancy on hydroxide ion rotation is dominant. We also note that the initial and final states have different energies, especially for systems with an A ion vacancy, implying that the proton is preferentially confined to a certain site. This is due to the A ion vacancy resulting in a relatively larger free space near some oxide ions, making these oxide ions more favorable acceptors than others. As shown in Fig. S2, the hydroxide ion in the initial BZY structure with one A ion vacancy (BZY-1Ba) is oriented towards the vacancy due to the free space. The larger free space in BZY with two A ion vacancies (BZY-2Ba) facilitates the hydroxide ion rotation between these two A ion vacancies because of the lower energy barrier as shown in Fig. 4a (blue curve with reaction coordinate smaller than 0.4). However, for longer range hydroxide ion rotation, the energy barrier is significant, similar to that of BZY with one A ion vacancy.

To gain an in-depth understanding of the role of an A ion vacancy on hydroxide ion rotation in perovskite oxides, we performed systematic DFT calculations on the three elementary steps underlying the hydroxide ion rotation for the two systems (one A ion vacancy and two A ion vacancy cases). The relative energies for the three steps are shown in Fig. 5a, b, and c, respectively. For comparison, we also show the relative energies for the system with no A ion vacancy. From the inset figure of Fig. 5a, we notice that the initial Zr-O_D (red O)-Zr' is deformed towards the A ion vacancy. Thus, compared to the O-B-O bending motion in the system with no A ion vacancies, there is a B-O_D-B bending motion in the systems with A ion vacancies, leading to a larger bending angle. The B-O-B bending motion structures are plotted in Fig. 1 (top right and bottom right) for comparison between systems with or without an A ion vacancy. For the hydroxide ion reorientation process (Fig. 5b), the system with an A ion vacancy shows a significantly higher energy barrier than the system with no A ion vacancies. Similarly, the relative energy increases to a maximum when the hydroxide ion rotates towards the Ba atom, but the relative energy decreases to a smaller value when the hydroxide ion rotates to the final position. Three systems (ideal structure with no A ion vacancies, one A ion vacancy, and two A ion vacancies) show similar trend of relative energy with no energy barrier for the lattice relaxation process (Fig. 5c). For both O-B-O bending motion and hydroxide ion reorientation, the two systems (one A ion vacancy and two A ion vacancy cases) exhibit larger energy barriers than the system with no A ion vacancy, which will be further explained in section 3.5. For the systems with A ion vacancies, the energy barriers for hydroxide ion rotation based on its decomposition into two processes (O-B-O outward bending and hydroxide ion reorientation) are consistent with the NEB calculated result as shown in Fig. 2b.

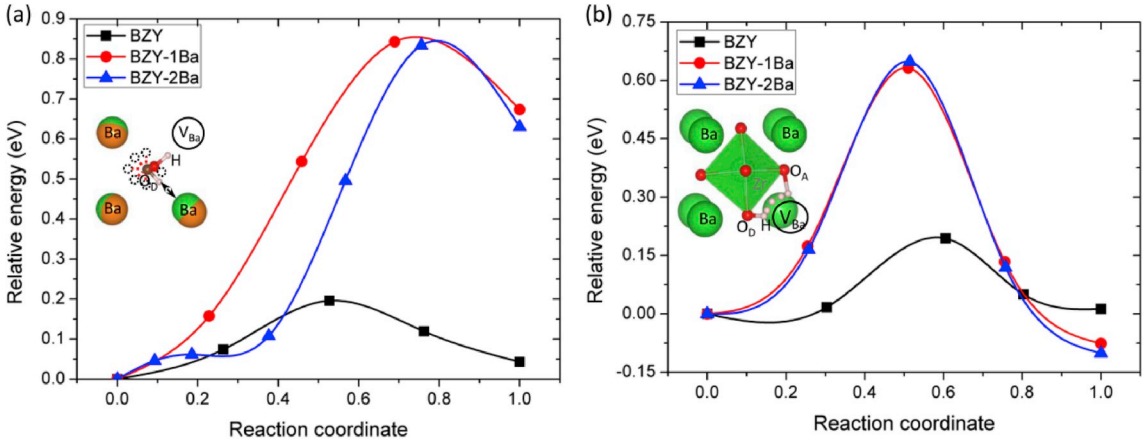

Fig. 4. Energy barrier associated with (a) hydroxide ion rotation in the AO plane and (b) proton transfer in three systems (BZY: ideal structure with no A ion vacancies, BZY-1Ba: one A ion vacancy, and BZY-2Ba: two A ion vacancies).

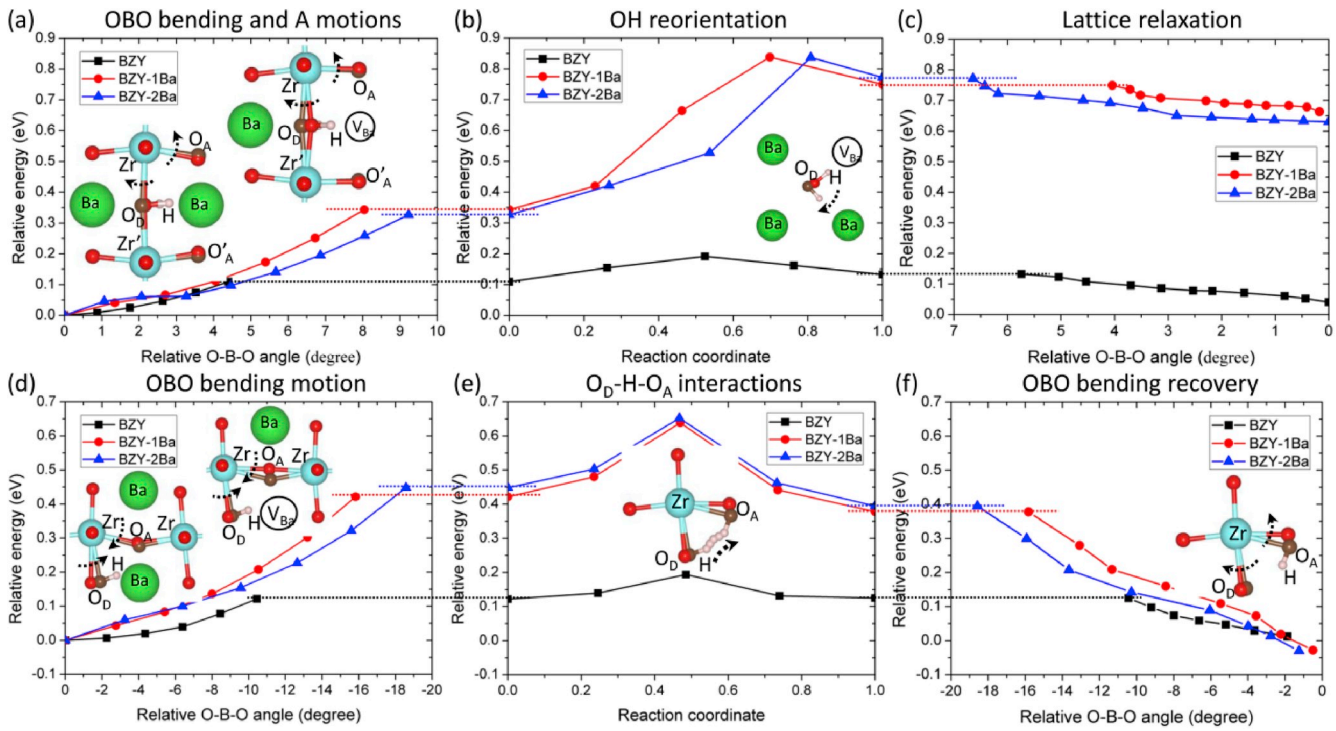

Fig. 5. Three elementary steps underlying the hydroxide ion rotation and proton transfer in the three systems (BZY: perfect lattice with no A ion vacancy, BZY-1Ba: one A ion vacancy, and BZY-2Ba: two A ion vacancies). (a) Relative energy with the O-B-O bending angle (∠ O_DBO_A of inset figure) during the outward O-B-O bending and A ion motions. (b) Relative energy with hydroxide ion reorientation in AO plane. (c) Relative energy with the O-B-O bending angle (∠ O_DZrO_C in Fig. S2) during lattice relaxation. (d) Relative energy with the O-B-O bending angle (∠ O_DBO_A of inset figure) during the inward O-B-O bending. (e) Relative energy for O_D-H-O_A interactions. (f) Relative energy with the O-B-O bending angle (∠ O_DBO_A of inset figure) during the recovery of the O-B-O bending motion. Inset figures show the local lattice deformation of saddle structure compared to initial structure. The red balls denote the initial positions and the brown balls show the final positions. (For interpretation of the references to colour in this figure legend, the reader is referred to the Web version of this article.)

3.4. Role of A-site ions on proton transfer

NEB calculations are performed to estimate the energy barriers for a proton transfer in the three systems (ideal structure with no A ion vacancies, one A ion vacancy, and two A ion vacancies) shown in Fig. S1. The relative energy in the NEB trajectories (see the snapshots in Fig. S4) are shown in Fig. 4b. The results show that the energy barriers for the proton transfer near an A ion vacancy are significantly higher than that in the perfect lattice. To confirm this result, the possible oxygen acceptors for a proton transfer near or far away from dopants (shown in Fig. S5) are considered. The energy barriers are summarized in Table S1. We note that an energy barrier range of 0.59–1.26 eV for a proton transfer near an A ion vacancy is larger than that of for the perfect lattice, which is consistent with experimental result [25]. We can thus conclude that the effect of A ion vacancy on proton transfer is significant.

To gain an in-depth understanding of the role of an A ion vacancy on proton transfer in perovskite oxides, we performed systematic DFT calculations on the elementary reactions underlying proton transfer for the two systems (one A ion vacancy and two A ion vacancy cases). The relative energies for the three steps are shown in Fig. 5d, e, and f. For comparison, we also show the relative energies for the system with no A ion vacancies. From the inset figure of Fig. 5d, we notice that the initial Zr-O_A (red O)-Zr is deformed further away from the A ion vacancy. Thus, compared to the O-B-O bending motion in the system with no A ion vacancies, there is a B-O_A-B bending motion in the systems with A ion vacancies, leading to a larger bending angle. For the O_D-H-O_A interaction process (Fig. 5e), the systems with A ion vacancies show a significantly higher energy barrier compared to the system with no A ion vacancies. The relative energy is maximum when the proton is in the middle of line connecting O_D and O_A, and decreases as proton approaches O_A. All the three systems show similar trends of relative energy with no energy barrier during the O-B-O bending recovery process (Fig. 5f). For both O-B-O bending motion and O_D-H-O_A interaction, the two systems (one A ion vacancy and two A ion vacancy cases) exhibit larger energy barriers than the system with no A ion vacancy, which will be further explained in section 3.5. For the systems with A ion vacancies, the energy barriers for proton transfer based its decomposition into first two processes are consistent with the NEB results as shown in Fig. 2d.

3.5. Effect of A-site ions on proton diffusion

From the results on the role of A-site ions on both hydroxide ion rotation and proton transfer, we observe that the systems with A ion vacancies have a larger relative energy than the systems with no A ion vacancies during the O-B-O bending process, hydroxide ion reorientation or during the O_D-H-O_A interaction process. Thus, to further understand the effect of A ion vacancy on hydroxide ion rotation and proton transfer, we investigate the effect of bond deformation on the O-B-O bending motion in both hydroxide ion rotation and proton transfer. As shown in Fig. 5a, four B-O bonds are involved in the O-B-O bending motion. For the hydroxide ion rotation process, one A-O bond is involved as well. We computed bond order [35], instead of bond strength, to understand the lattice deformation properties. The results of bond order together with energy barriers associated with O-B-O bending motion during hydroxide ion rotation or proton transfer for BZY systems with or without A ion vacancies are summarized in Table 1. As expected, a perfect BZY, with smaller barriers for O-B-O bending motion during hydroxide ion rotation or proton transfer, has smaller O-B bond orders, while BZY-1Ba (one A ion vacancy) and BZY-2Ba (two A ion vacancies), with larger barriers for O-B-O bending motion during hydroxide ion rotation or proton transfer, have larger O-B bond orders. Therefore, the

Table 1
Calculated bond orders.

System	Barrier (eV)		Bond order				
	O-B-O bending in OH rotation	O-B-O bending in proton transfer	O_D-Zr	O_D-Zr'	O_A-Zr	O_A-Zr'	O_D-Ba
BZY	0.1	0.12	0.31	0.34	0.48	0.48	0.06
BZY-1Ba	0.34	0.42	0.34	0.35	0.54	0.57	0.11
BZY-2Ba	0.33	0.45	0.36	0.37	0.57	0.60	0.09

presence of A ions reduces the bond strength between an oxygen and B ion. The reduced bond strength lowers the energy barrier for local structural deformations such as O-B-O bending and OA stretching motions, which facilitate both hydroxide ion rotation and proton transfer. The importance of the B-O strength for the proton diffusion was recently discussed in experimental work [17]. It was reported that the Ce-O stretching mode drives the proton diffusion with the coupling of the low-energy phonon mode. In addition, the influence of local lattice distortions on proton diffusion was discussed in recent work [37]. Localized polaronic lattice distortions can be condensed to trap the proton as the local dopant density increases. High-throughput ab initio calculation [38] found that $SrZrO_3$ is more difficult to dope than $BaZrO_3$ on the basis of the defect energies. Our calculations along with the published research validate the importance of A-site ions on B-O strengths in perovskite oxide for fast proton transport. Thus, perovskite oxides with A ions facilitate proton transport easily compared to other solid oxides without A ions, such as metal trioxides.

Next, we investigate the electronic density distribution (see Fig. 6) of the valence electrons of Zr, Ba and O atoms near the hydroxide ion reorientation during the hydroxide ion rotation process and O_D-H-O_A interactions during the proton transfer process. As shown in Fig. 6a, the

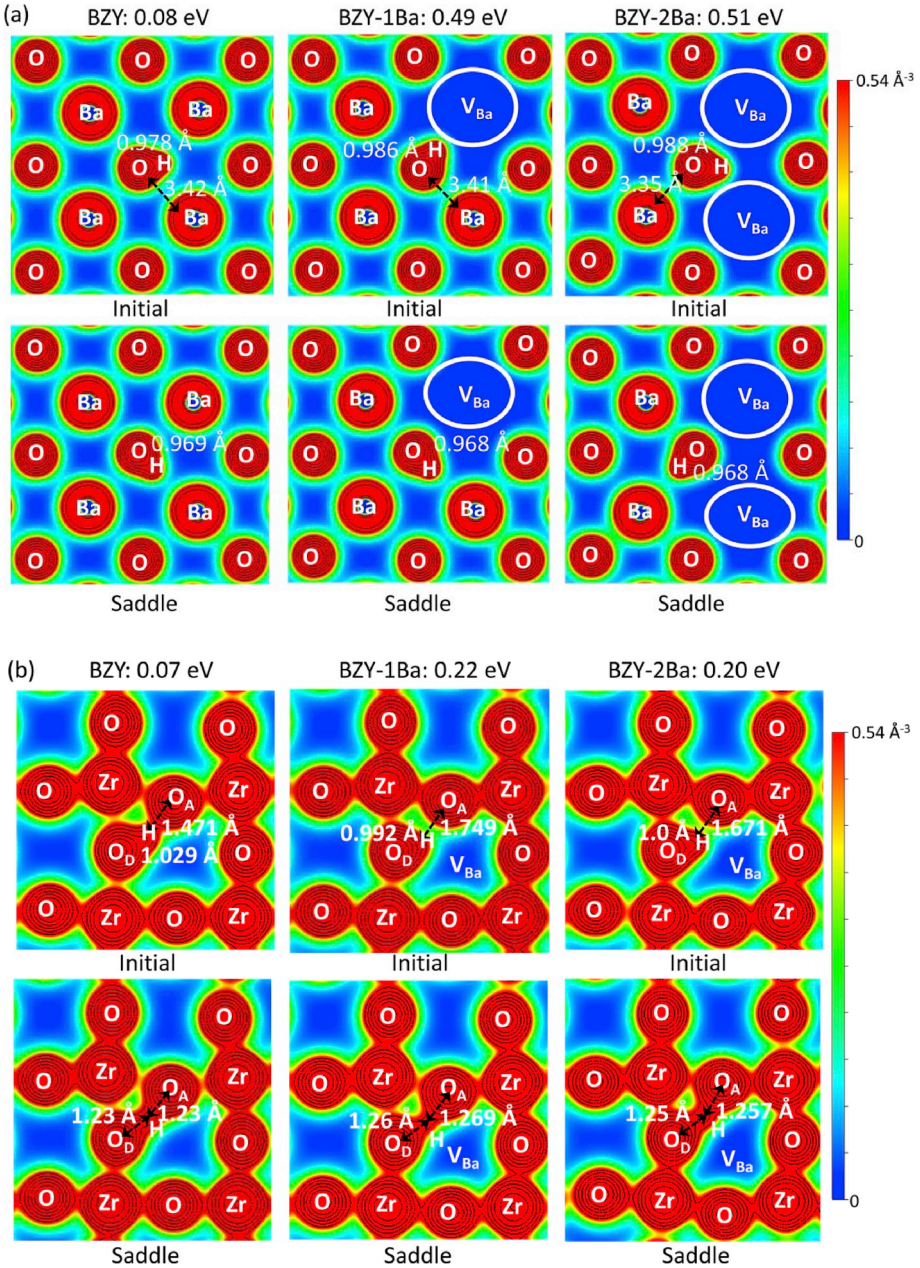

Fig. 6. Electronic density distribution for (a) hydroxide ion reorientation process of hydroxide ion rotation and (b) O_D-H-O_A interactions during proton transfer.

hydroxide ion bond length increases from 0.978 Å to 0.986 Å and 0.988 Å for BZY-1Ba and BZY-2Ba, respectively, due to the larger free space for proton provided by the A ion vacancy. In addition, an A ion vacancy increases the bond strength between oxygen and nearby A ion in terms of O-Ba bond length (3.42 Å, 3.41 Å, and 3.35 Å for BZY, BZY-1Ba, and BZY-2Ba, respectively). Thus, with A ion vacancies, the larger hydroxide ion bond length and the stronger O-A bond inhibit hydroxide ion reorientation and leads to a larger barrier for hydroxide ion reorientation during the hydroxide ion rotation process. As for the O_D-H-O_A interactions during the proton transfer process (shown in Fig. 6b), the A ion vacancy increases the bonding strength of proton with O donor (H-O bond lengths of 1.029 Å, 0.992 Å, and 1.0 Å for BZY, BZY-1Ba, and BZY-2Ba, respectively) and decreases the bonding strength of proton with O acceptor (H-O bond lengths of 1.471 Å, 1.749 Å, and 1.671 Å for BZY, BZY-1Ba, and BZY-2Ba, respectively), inhibiting O_D-H-O_A interactions due to the longer H-O_D bonds in BZY-1Ba and BZY-2Ba at the saddle state (H-O bond lengths of 1.23 Å, 1.26 Å, and 1.25 Å for BZY, BZY-1Ba, and BZY-2Ba, respectively). As shown in Fig. S4, the proton transfer trajectory is bent towards the edge of the octahedron as the edge of the octahedron provides the largest possibility of finding the negatively charged electrons, thus, attracting the proton with positive charge, as shown for the saddle state in Fig. 6b.

4. Conclusions

In this paper, we performed DFT calculations to reveal the role and significance of A-site ions on proton diffusion in perovskite oxides. We found that the presence of A-site ions reduces the barrier for proton diffusion, which includes hydroxide ion rotation and proton transfer mechanisms, demonstrating the significance of a perovskite structure as a proton conductor in comparison with metal trioxides which do not contain A-site ions and exhibit larger barriers for proton diffusion.

Proton diffusion is understood as a two-step mechanism consisting of hydroxide ion rotation and proton transfer – specifically, the outward O-B-O bending and A ion motions and hydroxide ion reorientation govern the hydroxide ion rotation process while the inward O-B-O bending motion and donor oxygen – proton – acceptor oxygen interactions govern the proton transfer process. The presence of A ions reduces the bond strength between O and B ions, thereby reducing the energy barrier for local lattice deformations such as the O-B-O bending motion, which plays an important role in both hydroxide ion rotation and proton transfer processes. In addition, the presence of A ions decreases the bonding strength of proton with donor oxygen and increases the bonding strength of proton with acceptor oxygen, promoting proton motion from donor oxygen to acceptor oxygen. Although an A ion vacancy provides a larger free space for proton, which favors hydroxide ion rotation within this free space (small angle rotation), it also increases the bond strength between oxygen and an adjacent A ion which proton needs to overcome for hydroxide ion rotation, thus inhibiting hydroxide ion reorientation motion with large angle rotations. While this work provides a thorough atomistic understanding of the role of A-site ions on proton diffusion in perovskite oxides, the results presented here can enable design and discovery of novel materials with improved proton diffusion properties.

Acknowledgements

This work is supported by the National Science Foundation under grant # 1545907, the National Center for Supercomputing Applications (NCSA), the NSF of China under Grant No. 11932005 and 11432005, and the International Postdoctoral Exchange Fellowship Program of China under Grants No. 20140016. This research is part of the Blue Waters sustained-petascale computing project, which is supported by the National Science Foundation (awards OCI-0725070 and ACI-1238993) and the state of Illinois. Blue Waters is a joint effort of the University of Illinois at Urbana-Champaign. The authors also acknowledge the use of the Extreme Science and Engineering Discovery Environment (XSEDE).

Appendix A. Supplementary data

Supplementary data to this article can be found online at https://doi.org/10.1016/j.jpowsour.2019.227327.

References

[1] T. Ishihara (Ed.), Perovskite Oxide for Solid Oxide Fuel Cells, Springer Science and Business Media, Dordrecht, The Netherlands, 2009.
[2] K. Ueda, H. Tabata, T. Kawai, Coexistence of ferroelectricity and ferromagnetism in $BiFeO_3$-$BaTiO_3$ thin films at room temperature, Appl. Phys. Lett. 75 (1999) 555.
[3] I. Kanno, S. Fujii, T. Kamada, R. Takayama, Piezoelectric properties of c-axis oriented $Pb(Zr,Ti)O_3$ thin films, Appl. Phys. Lett. 70 (1997) 1378.
[4] Y. Yamazaki, R. Hernandez-Sanchez, S.M. Haile, High total proton conductivity in large-grained yttrium-doped barium zirconate, Chem. Mater. 21 (2009) 2755–2762.
[5] Y. Teraoka, H.M. Zhang, K. Okamoto, N. Yamazoe, Mixed ionic-electronic conductivity of $La_{1-x}Sr_xCo_{1-y}Fe_yO_3$ perovskite-type oxides, Mater. Res. Bull. 23 (1988) 51–58.
[6] F.S. Galasso, Perovskites and High-T_c Superconductors, Gordon and Breach Science Pub, London, 1990.
[7] S.P.S. Badwal, Stability of solid oxide fuel cell components, Solid State Ion. 143 (2001) 39–46.
[8] R. Spinicci, M. Faticanti, P. Marini, S. De Rossi, P. Porta, Catalytic activity of $LaMnO_3$ and $LaCoO_3$ perovskites towards VOCs combustion, J. Mol. Catal. A Chem. 197 (2003) 147–155.
[9] D.J.L. Brett, A. Atkinson, N.P. Brandon, S.J. Skinner, Intermediate temperature solid oxide fuel cells, Chem. Soc. Rev. 37 (2008) 1568–1578.
[10] K.D. Kreuer, Proton-conducting oxides, Annu. Rev. Mater. Res. 33 (2003) 333–359.
[11] L. Bi, S. Boulfrad, E. Traversa, Steam electrolysis by solid oxide electrolysis cells (SOECs) with proton-conducting oxides, Chem. Soc. Rev. 43 (2014) 8255–8270.
[12] D. Pergolesi, E. Fabbri, A. D'Epifanio, E.D. Bartolomeo, A. Tebano, S. Sanna, S. Licoccia, G. Balestrino, E. Traversa, High proton conduction in grain-boundary-free yttrium-doped barium zirconate films grown by pulsed laser deposition, Nat. Mater. 9 (2010) 846–852.
[13] K.D. Kreuer, A. Fuchs, J. Maier, H/D isotope effect of proton conductivity and proton conduction mechanism in oxides, Solid State Ion. 77 (1995) 157–162.
[14] W. Münch, K.D. Kreuer, G. Seifertli, J. Majer, A quantum molecular dynamics study of proton diffusion in $SrTiO_3$ and $CaTiO_3$, Solid State Ion. 125 (1999) 39–45.
[15] Y. Yamazaki, F. Blanc, Y. Okuyama, L. Buannic, J.C. Lucio-Vega, C.P. Grey, S. M. Haile, Proton trapping in yttrium-doped barium zirconate, Nat. Mater. 12 (2013) 647–651.
[16] B. Merinov, W. Goddard III, Proton diffusion pathways and rates in Y-doped BaZrO3 solid oxide electrolyte from quantum mechanics, J. Chem. Phys. 130 (2009), 194707.
[17] A. Braun, Q. Chen, Experimental neutron scattering evidence for proton polaron in hydrated metal oxide proton conductors, Nat. Commun. 8 (2017), 15830.
[18] K.D. Kreuer, Aspects of the formation and mobility of protonic charge carriers and the stability of perovskite-type oxides, Solid State Ion. 125 (1999) 285–302.
[19] T.S. Bjørheim, A. Løken, R. Haugsrud, On the relationship between chemical expansion and hydration thermodynamics of proton conducting perovskites, J. Mater. Chem. A 4 (2016) 5917–5924.
[20] Y. Yamazaki, P. Babilo, S.M. Haile, Defect chemistry of yttrium-doped barium zirconate: a thermodynamic analysis of water uptake, Chem. Mater. 20 (2008) 6352–6357.
[21] A. Slodczyk, P. Colomban, S. Willemin, O. Lacroix, B. Sala, Indirect Raman identification of the proton insertion in the high-temperature [Ba/Sr][Zr/Ti]O_3-modified perovskite protonic conductors, J. Raman Spectrosc. 40 (2009) 513–521.
[22] A.L. Samgin, Lattice-assisted proton motion in perovskite oxides, Solid State Ion. 136 (2000) 291–295.
[23] V.V. Krasnoholovets, P.A. Tomchuk, S.P. Lukyanets, Proton transfer and coherent phenomena in molecular structures with hydrogen bonds, Adv. Chem. Phys. 125 (2003) 351–548.
[24] K.D. Kreuer, On the complexity of proton conduction phenomena, Solid State Ion. 136–137 (2000) 149–160.
[25] Y. Yamazaki, R. Hernandez-Sanchez, S.M. Haile, Cation non-stoichiometry in yttrium-doped barium zirconate: phase behavior, microstructure, and proton conductivity, J. Mater. Chem. 20 (2010) 8158–8166.
[26] G.C. Mather, S. García-Martín, D. Benne, C. Ritter, U. Amador, A-site-cation deficiency in the $SrCe_{0.9}Yb_{0.1}O_{3-\delta}$ perovskite: effects of charge-compensation mechanism on structure and proton conductivity, J. Mater. Chem. 21 (2011) 5764–5773.
[27] Y. Jing, H. Matsumoto, N.R. Aluru, Mechanistic insights into hydration of solid oxides, Chem. Mater. 30 (2018) 138–144.
[28] G. Kresse, J. Furthmüller, Efficiency of ab-initio total energy calculations for metals and semiconductors using a plane-wave basis set, Comput. Mater. Sci. 6 (1996) 15–50.
[29] G. Kresse, D. Joubert, From ultrasoft pseudopotentials to the projector augmented-wave method, Phys. Rev. B Condens. Matter Mater. Phys. 59 (1999) 1758.

[30] G. Kresse, J. Furthmuller, Efficient iterative schemes for ab initio total-energy calculations using a plane-wave basis set, Phys. Rev. B Condens. Matter Mater. Phys. 54 (1996), 11169.
[31] J.P. Perdew, K. Burke, M. Ernzerhof, Generalized gradient approximation made simple, Phys. Rev. Lett. 77 (1996) 3865.
[32] G. Henkelman, B.P. Uberuaga, H. Jónsson, A climbing image nudged elastic band method for finding saddle points and minimum energy paths, J. Chem. Phys. 113 (2000) 9901–9904.
[33] M.A. Gomez, M.A. Griffin, S. Jindal, K.D. Rule, V.R. Cooper, The effect of octahedral tilting on proton binding sites and transition states in pseudo-cubic perovskite oxides, J. Chem. Phys. 123 (2005), 094703.
[34] P.G. Sundell, M.E. Björketun, G. Wahnström, Density-functional calculations of prefactors and activation energies for H diffusion in $BaZrO_3$, Phys. Rev. B 76 (2007), 094301.
[35] T.A. Manz, Introducing DDEC6 atomic population analysis: part 3. Comprehensive method to compute bond orders, RSC Adv. 7 (2017), 45552.
[36] C.J. T.d. Grotthuss, Mémoire sur la décomposition de l'eau et des corps qu'elle tient en dissolution à l'aide de l'électricité galvanique, Ann. Chim. 58 (1806) 54–74.
[37] J. Ding, J. Balachandran, X. Sang, W. Guo, J.S. Anchell, G.M. Veith, C.A. Bridges, Y. Cheng, C.M. Rouleau, J.D. Poplawsky, N. Bassiri-Gharb, R.R. Unocic, P. Ganesh, The influence of local distortions on proton mobility in acceptor doped perovskites, Chem. Mater. 30 (2018) 4919–4925.
[38] J. Balachandran, L. Lin, J.S. Anchell, C.A. Bridges, P. Ganesh, Defect genome of cubic perovskites for fuel cell applications, J. Phys. Chem. C 121 (2017) 26637–26647.
[39] A.B. Muñoz-García, M. Pavone, First-principles design of new electrodes for proton-conducting solid-oxide electrochemical cells: a-site doped $Sr_2Fe_{1.5}Mo_{0.5}O_{6-\delta}$ perovskite, Chem. Mater. 28 (2016) 490–500.
[40] J.A. Dawson, J.A. Miller, I. Tanaka, First-principles insight into the hydration ability and proton conduction of the solid state proton conductor, Y and Sn co-doped $BaZrO_3$, Chem. Mater. 27 (2015) 901–908.
[41] Ph Colomban, Latest developments in proton conductors, Ann. Chim. Sci. Mat 24 (1999) 1–18.
[42] Ph Colomban, C. Tran, O. Zaafrani, A. Slodczyk, Aqua oxyhydroxycarbonate second phases at the surface of Ba/Sr-based proton conducting perovskites: a source of confusion in the understanding of proton conduction, J. Raman Spectrosc. 44 (2013) 312–320.
[43] A. Slodczyk, M.D. Sharp, S. Upasen, P. Colomban, J.A. Kilner, Combined bulk and surface analysis of the $BaCe_{0.5}Zr_{0.3}Y_{0.16}Zn_{0.04}O_{3-\delta}$ (BCZYZ) ceramic proton-conducting electrolyte, Solid State Ion. 262 (2014) 870–874.
[44] Ph Colomban, J. Tomkinson, Novel forms of hydrogen in solids: the 'ionic' proton and the 'quasi-free' proton, Solid State Ion. 97 (1997) 123–134.
[45] S. Deng, Y. Zhang, Location and lattice dynamics of a proton in the perovskite structure, Phys. Status Solidi B 253 (2016) 1688–1696.
[46] Ph Colomban, Proton conductors and their applications: a tentative historical overview of the early researches, Solid State Ion. 334 (2019) 125–144.
[47] Ph Colomban, A. Slodczyk, The structural and dynamics neutron study of proton conductors: difficulties and improvement procedures in protonated perovskite, Eur. Phys. J. Spec. Top. 213 (2012) 171–193.
[48] A. Slodczyk, Ph Colomban, G. André, O. Zaafrani, F. Grasset, O. Lacroix, B. Sala, Structural modifications induced by free protons in proton conducting perovskite zirconate membrane, Solid State Ion. 225 (2012) 214–218.
[49] D. Shima, S.M. Haile, The influence of cation non-stoichiometry on the properties of undoped and gadolinia-doped barium cerate, Solid State Ion. 97 (1997) 443–455.
[50] C.W. Myung, J. Yun, G. Lee, K.S. Kim, A new perspective on the role of A-site cations in perovskite solar cells, Adv. Energy Mater. 8 (2018), 1702898.
[51] K.K. Hansen, Studies of A-site deficient $(Gd_{0.6}Sr_{0.4})_{1-\delta}Fe_{0.8}Co_{0.2}O_{3-\delta}$ cathodes in SOFCs, Fuel Cells 18 (2018) 96–100.
[52] H. Kumomi, F.G. Shi, Direct measurement of the free-energy barrier to nucleation from the size distribution of dendritic crystallites in *a*-Si thin films, Phys. Rev. B 52 (1995), 16753.
[53] P. Gorai, E.G. Seebauer, E. Ertekin, Mechanism and energetics of O and O2 adsorption on polar and non-polar ZnO surfaces, J. Chem. Phys. 144 (2016), 184708.
[54] K. Kreuer, Proton conductivity: materials and applications, Chem. Mater. 8 (1996) 610–641.